

Addressing Model and Data Heterogeneity in Multimodal Large Language Model Training

Zili Zhang*

Yinmin Zhong*

Ranchen Ming[†]Hanpeng Hu[†]Jianjian Sun[†]Zheng Ge[†]Yibo Zhu[†]

Xin Jin*

^{*}Peking University[†]StepFun

Abstract

Multimodal large language models (LLMs) have demonstrated significant potential in a wide range of AI applications. Yet, training multimodal LLMs suffers from low efficiency and scalability, due to the inherent model heterogeneity and data heterogeneity across different modalities.

We present MMScale, an efficient and adaptive framework to reform the training of multimodal large language models on large-scale clusters. MMScale exploits the system characteristics of multimodal LLM training to achieve high efficiency and scalability. The core of MMScale is the adaptive resource allocation and data-aware reordering techniques to eliminate the model and data heterogeneity respectively. We also tailor system optimizations for multimodal LLM training to offload certain operations from the GPU training. We evaluate MMScale across different sizes of multimodal LLMs on a large-scale production cluster with thousands of GPUs. The experimental results show that MMScale achieves 54.7% Model FLOPs Utilization (MFU) when training a 72B multimodal LLM on 1172 GPUs and outperforms Megatron-LM by up to 2.2 \times on throughput. The ablation study shows the main techniques of MMScale are both effective and lightweight.

1 Introduction

Recent advances in large language models (LLMs) are catalyzing a new wave of AI applications [1]. However, LLMs are predominantly text-based, restricting their ability to understand and generate multimodal content. Emerging multimodal LLMs address this gap by integrating various modalities such as texts, images, and audios into LLMs which significantly enhances LLM's applicability. Multimodal LLMs demonstrate great potential in tasks like image understanding [2–5], audio comprehension [6, 7], and embodied AI [8, 9]. Many organizations are actively developing their multimodal LLMs, such as OpenAI's GPT-4o [10], Google's Gemini [11] and PaLM-E [9], Meta's Chameleon [12], etc.

Training multimodal LLMs demands vast computational resources. According to the scaling law [13], model size and training data volume are crucial for determining model capabilities. Substantial efforts are invested in training models with billions of parameters on trillion-scale tokens. For instance, Meta's Chameleon [12] is a 34B multimodal LLM

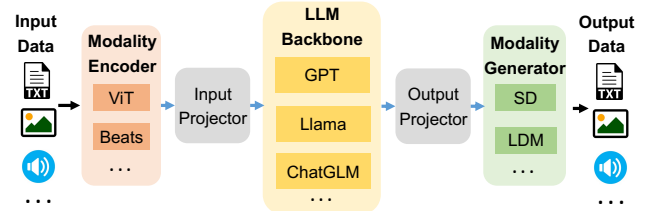


Figure 1: The architecture of multimodal LLMs.

trained on more than 4.8 trillion tokens. Leading organizations often deploy large-scale clusters, equipped with thousands of GPUs, for such training tasks. One technical report [14] reveals that training a GPT-3 175B with 300 billion tokens costs \$4.6 million and lasts one year using 355 V100 GPUs. Consequently, it is crucial to develop an efficient and scalable training framework to minimize costs and accelerate training.

Figure 1 depicts the mainstream model architecture of multimodal LLMs, comprising three primary modules: the modality encoder, LLM backbone, and the modality generator [15, 16]. These modules are linked by the projector, which may incorporate MLP or cross-attention layers. The modality encoder transforms input from various modalities into a unified embedding space. The embedding vectors are then analyzed by the LLM backbone, a transformer model, to discern data patterns and inter-modal relationships. Subsequently, the modality generator translates this processed information back into coherent outputs tailored to each modality.

Megatron-LM [17] is the state-of-the-art framework for training LLMs, which comprise a stack of homogeneous transformer layers. It can be extended to train multimodal LLMs by treating the multimodal modules as additional layers within the LLM. However, training multimodal LLMs with Megatron-LM poses two substantial challenges: *model heterogeneity* and *data heterogeneity*. The fundamental issue of model heterogeneity stems from the need to process diverse modalities with different modules that vary dramatically in size and operator complexity. The model heterogeneity across different modules (i.e., modality encoder, LLM backbone, and modality generator) introduces severe pipeline bubbles, resulting in poor GPU utilization. Meanwhile, data heterogeneity bursts onto the scene due to the intricate and unstructured nature of multimodal input data. The data heterogeneity across different modality data leads to inter-microbatch

and intra-microbatch training stragglers, which prolong the training duration and exacerbate the pipeline bubbles. These challenges collectively limit the efficiency and scalability of multimodal LLM training, resulting in MFU as low as $\sim 20\%$ in production-level training (§7.1).

To this end, we present MMScale, an efficient and adaptive framework to reform the training of multimodal LLMs. MMScale achieves state-of-the-art MFU which is close to unimodal (i.e., text-only) LLM training and effectively scales to large clusters with thousands of GPUs. The core of MMScale is adaptive resource allocation and data-aware reordering. These two techniques leverage the distinctive system characteristics of multimodal LLM training to eliminate model heterogeneity and data heterogeneity respectively.

For model heterogeneity, we meticulously analyze the pipeline bubbles stemming from model heterogeneity and identify their root causes (§2.2). Based on this analysis, we propose disaggregated training, which tailors the resource allocation and parallelism strategies across the modality encoder, LLM backbone, and modality generator. We also develop a novel and lightweight algorithm to navigate this complicated design space to choose the optimal resource and parallelism configurations. This innovative approach minimizes the pipeline bubbles and achieves optimal training efficiency.

For data heterogeneity, we categorize the training stragglers into inter-microbatch and intra-microbatch stragglers (§2.3) and introduce tailored algorithms that strategically reorder training data while maintaining synchronous training semantics. The inter-microbatch reordering algorithm reorders the data samples to evenly distribute the load across different data parallelism groups. The intra-microbatch reordering algorithm reorders the microbatches tailored for (interleaved) 1F1B pipeline scheme to minimize the pipeline bubbles. This two-level approach effectively mitigates training stragglers caused by data heterogeneity.

In addition, we customize system optimizations for multimodal LLM training to offload certain operations from the critical path (i.e., GPU computation). We implement an asynchronous data loader to pre-process the training data with negligible runtime overhead. We implement an in-house collective communication library, StepCCL, to hide the communication overhead within the computation.

In summary, we make the following contributions.

- We present MMScale, an efficient and adaptive framework to reform the training of multimodal LLMs by harnessing the multimodal heterogeneity. It delivers state-of-the-art MFU on large-scale clusters with thousands of GPUs.
- We identify and discuss the primary challenges associated with multimodal LLM training, which are summarized as *model heterogeneity* and *data heterogeneity*.
- We implement disaggregated training across the three modules in multimodal LLMs. We propose adaptive resource allocation and data-aware reordering to effectively address model and data heterogeneity, respectively.

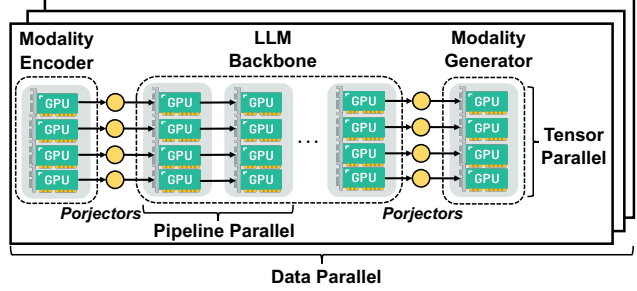


Figure 2: Training multimodal LLMs with Megatron-LM.

- We implement MMScale and conduct experiments on our production cluster with thousands of GPUs. The experimental results show that MMScale achieves 54.7% MFU when training a 72B multimodal LLM on 1172 GPUs and outperforms Megatron-LM by up to $2.2\times$ on throughput.

2 Motivation

2.1 Multimodal Large Language Model Training

Large language model. Large language models (LLMs) [18–20] have revolutionized natural language processing (NLP) by achieving state-of-the-art performance on a wide range of tasks, such as text generation, translation, and summarization. Many organizations have raced to develop their own LLMs, such as OpenAI’s GPT-4 [21], Google’s Gemini [11], and Meta’s Llama [22]. The core architecture of LLMs consists of a stack of homogeneous transformer layers [18] that use self-attention mechanisms to capture contextual information in text. LLMs are pre-trained with unsupervised learning on large-scale text corpora and then fine-tuned on task-specific text datasets. The text data is typically tokenized into fixed-length sequences, which are then fed into the model to learn the underlying patterns. The training process involves weeks or even months of computation on dedicated AI clusters with thousands of GPUs. According to one technical report [14], training 175B GPT-3 requires 4.6 million dollars. Optimizing the training process is essential to reduce the stupendous cost and accelerate the model deployment.

Multimodal LLM. The unimodal LLMs are limited to processing text data, which restricts their applicability to multimodal tasks (e.g., image understanding and generation). As a result, multimodal LLMs have emerged to address this limitation by integrating multiple modalities (e.g., images, audios, and videos) into the advanced LLMs [15], which support multimodal inputs and outputs during LLM generation. For example, GPT-4o [10] garners widespread attention by facilitating more natural interactions with humans through both visual and auditory modalities. Moreover, the predominantly text-based data in human societies is finite [23]. Harnessing multimodal data is inevitable to continually expand and enhance LLM capabilities.

Figure 1 illustrates the model architecture of a multimodal LLM, which consists of three modules: a modality encoder,

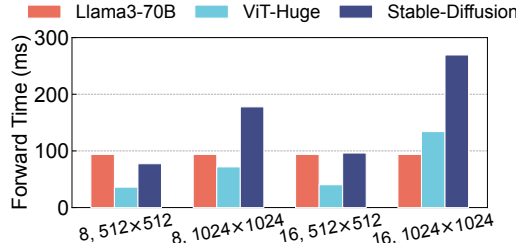


Figure 3: Forward time under different input configurations.

an LLM backbone, and a modality generator [15, 16, 24]. The modality encoder transforms input data from different modalities (e.g., ViT [25] for images and Beats [26] for audios) into an intermediate representation (i.e., an embedding tensor), which is then projected into a unified embedding space across modalities with input projection layers (e.g., MLP and cross-attention). The LLM backbone, typically a transformer model (e.g., GPT [19, 20] and Llama [22]), processes the multimodal embeddings to discern the intricate data patterns and inter-modal relationships. The output data of the LLM backbone is subsequently refined by output projection layers, which tailor the information for each modality. Finally, the modality generator (e.g., Diffusion [27] for images and Audioldm [28] for audios) transforms the LLM-processed information back into the respective modal outputs to generate coherent and contextually relevant results.

Multimodal LLM training necessitates training all three modules simultaneously. Additionally, during different training phases, specific modules are frozen to stabilize training loss and enhance model effectiveness [15]. Regarding the training data, the input sequence comprises text, image, and audio tokens. These data from different modalities are tokenized into *subsequences* which are then interleaved to form fixed-length training *sequences* [12]. In cases where the input sequence falls short, it is padded with zero tokens for batching. Distinct modality sub-sequences are demarcated by special tokens and processed through modality-specific encoders.

Training framework. To train the multimodal large language model with large-scale clusters, the de facto solution is to leverage Megatron-LM, a highly efficient and robust training framework for large-scale transformer models. Megatron-LM employs a unified parallelism strategy for the entire model. It combines tensor parallelism (TP) and pipeline parallelism (PP) to distribute the model parameters across multiple GPUs. TP divides the model parameter within each layer, while PP partitions parameters between layers. It also leverages data parallelism (DP) to distribute the training data. For multimodal LLMs, Megatron-LM is easily extended to integrate additional multimodal modules. Figure 2 illustrates the training topology of multimodal LLMs with Megatron-LM. Specifically, Megatron-LM treats the multimodal modules as additional layers within the LLM and incorporates additional PP stages to accommodate the modality encoder and generator. The same TP strategy used in the LLM backbone is applied

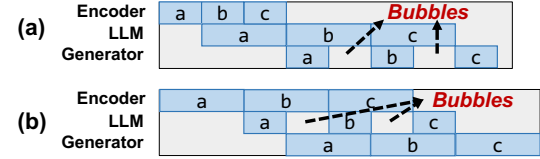


Figure 4: Two types of pipeline bubbles due to model heterogeneity.

to these two multimodal modules. If the modality encoder and generator are not large enough, they are replicated across the GPUs in the TP group to maximize resource utilization. As for DP, Megatron-LM applies the same DP strategy to the multimodal modules as the LLM backbone. The projector is co-located with the modality encoder and generator and is replicated across the GPUs in the TP group.

However, this training framework introduces significant computation imbalance stemming from *model heterogeneity* and *data heterogeneity* due to its rigid resource allocation method (i.e., the multimodal modules share the same DP and TP strategies with LLM backbone). It only achieves ~20% MFU (§7.1) which is significantly lower than the MFU of ~50% observed in training unimodal (text-only) LLMs [29].

2.2 Model Heterogeneity

The first challenge is the computation imbalance arising from model heterogeneity. Each module in multimodal LLMs bears different computational demands due to varying operators and inputs. For instance, ViT, as modality encoder, is constructed with narrow transformer layers (i.e., small hidden size), whereas LLM backbone is built on broader transformer layers (i.e., large hidden size). Meanwhile, Diffusion, as modality generator, utilizes a combination of convolution and attention layers (i.e., U-Net). This architectural diversity results in distinct computation time for each module. Figure 3 shows varying forward time under different input configurations with Megatron-LM. We demonstrate one PP stage of LLM backbone with PP size of 10 and TP size of 8. The first configuration parameter is the number of images in the 8K input sequence, and the second is the image resolution. The time differs markedly across different configurations.

The computational imbalance between modules leads to two types of pipeline bubbles in pipeline parallelism. The first arises in the modality encoder and generator stages, as shown in Figure 4(a), resulting from their inadequate utilization of assigned GPU resources. The second type emerges in the stages of the LLM backbone, as shown in Figure 4(b). This is because the intensive computational demands of the encoder and generator extend their stage durations. Due to the pipeline dependency, the LLM stages are forced to wait for the multimodal stage to complete, thereby creating pipeline bubbles. The latter problem is particularly pronounced during large-scale multimodal LLM training, where the bulk of GPU resources are allocated to the LLM backbone. These pipeline bubbles, stemming from model heterogeneity, substantially diminish the MFU during the training.

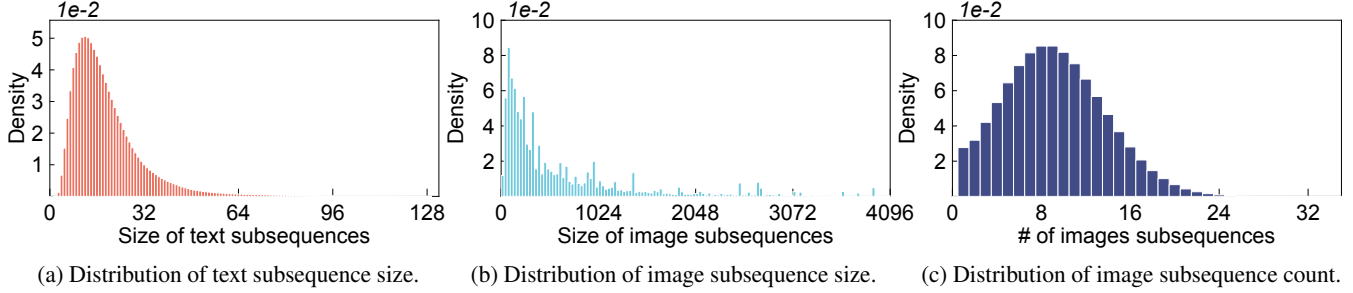


Figure 5: Data heterogeneity in multimodal LLM training.

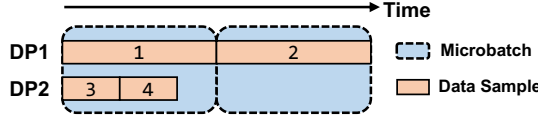


Figure 6: Intra-microbatch straggler (among DP groups).

2.3 Data Heterogeneity

The second challenge is the computational imbalance stemming from data heterogeneity. Each input sequence (i.e., training sample) for multimodal LLM training consists of interleaved modality subsequences that exhibit highly skewed distributions. Focusing on images and texts, we perform data characterization on the LAION-400M dataset [30], an open-source collection of images paired with text captions. Each image (i.e., one image subsequence) is segmented into 16×16 patches, and each patch is tokenized into one image token. The texts are tokenized through Llama tokenizer. The image tokens are interleaved with text tokens to create an 8K-token input sequence for training. As shown in Figure 5(a) and Figure 5(b), the sizes of text and image subsequences display distinctly skewed distributions. We further analyze the count of modality subsequence per training sample using image as an example. The count of image subsequences per training sample, shown in Figure 5(c), also demonstrates a skewed distribution. Different sample size (i.e., modality tokens per sample) leads to varying computation time in the modality encoder and generator stages.

Such data heterogeneity results in both *intra-microbatch* and *inter-microbatch* stragglers within the pipeline parallelism (PP) stages of the modality encoder and generator. These stragglers exacerbate the computational imbalances and further reduce the GPU utilization. It is noted that all microbatches within LLM backbone have the same computation time since the sequence length is fixed. We do not consider data heterogeneity between global batches, as each global batch contains numerous randomly shuffled training samples (e.g., thousands with a large DP size), which effectively smooths out the data heterogeneity.

Intra-microbatch straggler. Intra-microbatch straggler occurs when particularly large training samples decelerate training, as DP groups handle variably-sized training samples. Illustrated in Figure 6, the first DP group (*DP1*) processes two

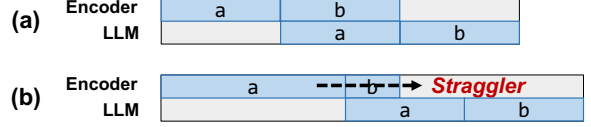


Figure 7: Inter-microbatch straggler.

large training samples within two microbatches. In contrast, the second DP group (*DP2*) processes two smaller samples in the same microbatches, completing them more swiftly. Consequently, *DP1* lags behind and becomes the straggler, which delays the overall training process.

Inter-microbatch straggler. Inter-microbatch straggler emerges from pipeline imbalances between microbatches. As depicted in Figure 7, the first pipeline stage is the modality encoder followed by one LLM backbone stage. Figure 7(a) illustrates the pipeline without data heterogeneity, where the modality encoder processes each microbatch with consistent time. In contrast, Figure 7(b) depicts the pipeline with data heterogeneity, where the forward time of the modality encoder varies markedly across microbatches. The straggler (i.e., the microbatch *a*) significantly delays the training process of the subsequent PP stages, leading to a large pipeline bubble.

3 MMScale Overview

We present MMScale, an efficient and adaptive framework to reform the training of multimodal LLMs by harnessing the multimodal heterogeneity. MMScale exploits the characteristics of parallelism training of multimodal LLMs to achieve high efficiency and scalability. MMScale eliminates the model heterogeneity by adaptive resource allocation (§4) and harnesses the data heterogeneity by data-aware reordering (§5). In addition, MMScale adopts some system optimizations tailored for multimodal LLM training (§6). Here we provide a brief overview of MMScale as Figure 8 shows.

MMScale orchestrator. Before training, MMScale employs a training orchestrator to determine the resource allocation and parallelism strategy for each module in multimodal LLMs. This scheduler first gathers the model architecture and training configuration (e.g., global batch size) from the user and randomly samples a subset of training data to analyze the data distribution. Utilizing this information, it runs a series of benchmarking training trials and constructs a performance

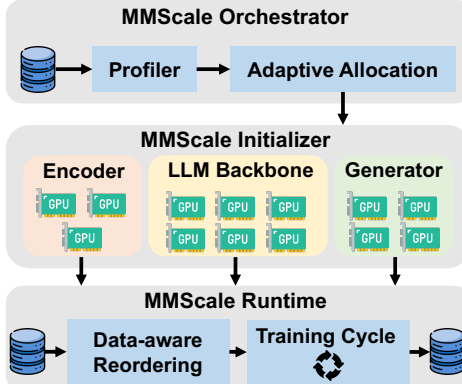


Figure 8: MMScale overview.

profiler with linear interpolation to estimate each module’s computation and communication time. Based on the profiling results, the training orchestrator decides the optimal resource allocation and parallelism strategy with *adaptive resource allocation* for one specific training task, as detailed in §4.

MMScale initializer. Then, MMScale initializes the parallelism units for the modality encoder, LLM backbone, and modality generator, respectively. MMScale allocates different numbers of GPUs to each unit. Each unit then establishes the communication group across different nodes and GPUs. The unit loads the model checkpoint from distributed file system and shards the model parameters and optimization states. Finally, MMScale conducts several communication trials to warm up the system and test connectivity.

MMScale runtime. After initialization, MMScale begins the main training process. In each training iteration, it first retrieves a global batch of training samples from the distributed file system for pre-processing. Then, MMScale performs *data-aware reordering* to reorder the training samples within one global batch without breaking the synchronous training semantics [31]. This module effectively eliminates both inter-microbatch and intra-microbatch data heterogeneity, as detailed in §5. The data then undergoes sequentially through the modality encoder, LLM backbone, and modality generator in the training pipeline. Finally, it synchronizes the gradients and model parameters through the all-gather operation, employing the ZERO-1 optimization [32] and mixed precision training [33]. Additionally, MMScale adopts a dedicated process to periodically and asynchronously save the model checkpoint to the distributed file system for fault tolerance.

4 Addressing Model Heterogeneity

Before diving into the details, we first introduce the disaggregation of the training across the three modules (i.e., modality encoder, LLM backbone, and modality generator) in multi-modal LLMs. This disaggregation facilitates adaptive GPU resource allocation among the different modules based on the training workload. Subsequently, we formulate the problem of adaptive resource allocation to minimize the training time

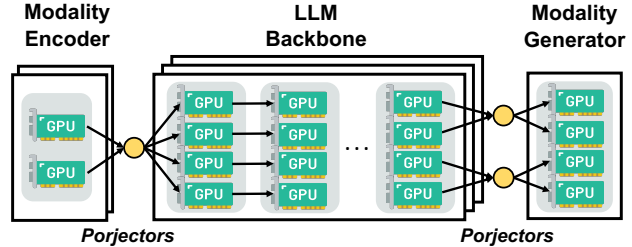


Figure 9: Disaggregated training in MMScale.

per iteration. Finally, we present the detailed algorithm to optimally address the problem caused by model heterogeneity.

4.1 Disaggregated Training

Disaggregating the training among the three modules is the foundation of adaptive resource allocation in MMScale. Figure 9 demonstrates the training topology of disaggregated training in MMScale. Different from the rigid resource allocation in Megatron-LM (i.e., Figure 2), MMScale is able to adaptively adjust the resource allocation. For instance, MMScale allocates 4 GPUs (DP=2 and TP=2) to the modality encoder, 12 GPUs (DP=3 and TP=4) to the LLM backbone per PP stage, and 4 GPUs (DP=1 and TP=4) to the modality generator. Additionally, the projector layers are colocated with either the modality encoder or generator, with their number of replicas adapting as needed. We implement the disaggregated training through a dedicated module, i.e., *parallelism unit*.

Parallelism unit. At training initialization, we need to establish the communication group according to the resource allocation and parallelism strategy. MMScale introduces a module, parallelism unit, composed of one or more PP stages. Each unit can adopt its own DP and TP strategies and form a specific communication group. Inter-unit connections are facilitated by a *communication broker*, which bridges PP communication across parallelism units. Users are only required to specify the DP and TP configurations for each parallelism unit, and MMScale automatically sets up the communication group and communication broker. MMScale treats the modality encoder, LLM backbone, and modality generator as three individual parallelism units. The detailed implementation of parallelism unit is discussed in §6.

4.2 Problem Formulation

With disaggregated training, we are able to adaptively allocate GPU resources across the three modules. The problem now lies in determining the optimal resource allocation and parallelism strategy to minimize the training time per iteration. Exhaust search is infeasible due to the large search space of the parallelism strategy and cluster size. One strawman solution is to allocate the GPU resources proportional to the model flops of each module. However, this method falls short as it overlooks complex patterns in parallelism training. For instance, different DP and TP sizes in modality encoder could lead to different computation times while the model flops are

the same. Before diving into the adaptive resource allocation algorithm, we first formulate the optimization problem.

LLM backbone. We begin by formulating the LLM backbone, focusing on the forward pass as the backward pass time mirrors this. In LLM training, microbatch size is set to one to prevent GPU memory overflow. Assume the global batch size for one iteration as BS and the TP size of the LLM backbone as TP_{lm} . Let the PP and DP size of LLM backbone be PP_{lm} and DP_{lm} . The number of GPUs allocated to LLM backbone is $y = TP_{lm} \times DP_{lm} \times PP_{lm}$. Let the forward time (including communication time) of the entire LLM be $C_{lm}(TP_{lm})$, where C_{lm} represents forward time function. Therefore, the forward time of one PP stage for one microbatch is $T_{lm} = \frac{C_{lm}(TP_{lm})}{\frac{BS}{DP_{lm}}}$. Besides, the number of microbatches per iteration is $\frac{BS}{DP_{lm}}$.

Modality encoder and generator. In MMScale, the modality encoder is regarded as a parallelism unit with PP size PP_{me} . Let the TP size be TP_{me} and the DP size be DP_{me} . The number of GPUs allocated to modality encoder is $x = TP_{me} \times DP_{me} \times PP_{me}$. The microbatch size is $\frac{DP_{lm}}{DP_{me}}$ which is determined by the LLM backbone. Let the forward time (including communication time) of the entire modality encoder be $C_{me}(TP_{me})$. The forward time of one PP stage for one microbatch in the modality encoder is $T_{me} = \frac{DP_{lm}}{DP_{me}} \times \frac{C_{me}(TP_{me})}{PP_{me}} = \frac{DP_{lm} \times TP_{me}}{x} \times C_{me}(TP_{me})$. Similarly, the forward time of one PP stage in the modality generator is $T_{mg} = \frac{DP_{lm} \times TP_{mg}}{z} \times C_{mg}(TP_{mg})$, where z is the number of GPUs allocated to modality encoder.

Objective function. Based on the preceding analysis, we next define the objective function for the optimization problem, i.e., the training time of one iteration. As shown in Figure 10, we demonstrate the pipeline of forward pass in multimodal LLM training. The LLM backbone comprises two PP stages, whereas the modality encoder and generator each consist of one PP stage. The training process is categorized into two phases: warm-up phase and steady phase. The warm-up phase spans from the initiation to the completion of the first microbatch to populate the pipeline. This phase's duration is calculated as $T_{warmup} = T_{lm} \times PP_{lm} + T_{me} \times PP_{me} + T_{mg} \times PP_{mg}$, which is formulated as follows.

$$T_{warm} = C_{lm}(TP_{lm}) + \frac{DP_{lm}}{DP_{me}} \times C_{me}(TP_{me}) + \frac{DP_{lm}}{DP_{mg}} \times C_{mg}(TP_{mg}) \quad (1)$$

The steady phase's duration is dominated by the maximal computation time among PP stages, which is calculated as $T_{steady} = \max(T_{lm}, T_{me}, T_{mg}) \times \left(\frac{BS}{DP_{lm}} - 1\right)$, where $\frac{BS}{DP_{lm}}$ is the number of microbatches per iteration. It is formulated as:

$$T_{steady} = \max \left\{ \frac{\frac{DP_{lm} \times TP_{lm}}{y} \times C_{lm}(TP_{lm})}{PP_{lm}}, \frac{\frac{DP_{lm} \times TP_{me}}{x} \times C_{me}(TP_{me})}{PP_{me}}, \frac{\frac{DP_{lm} \times TP_{mg}}{z} \times C_{mg}(TP_{mg})}{PP_{mg}} \right\} \times \left(\frac{BS}{DP_{lm}} - 1\right) \quad (2)$$

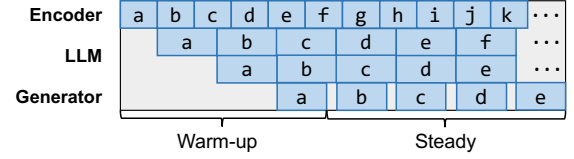


Figure 10: Multimodal LLM training pipeline.

Therefore, the objective function is to minimize $T_{iter} = T_{warmup} + T_{steady}$. For the backward pass, the objective function remains analogous to that of the forward pass. Adjustments are made by changing C_{lm} , C_{me} , and C_{mg} from forward time functions to the sum functions of forward and backward time. This formulation holds for GPipe and 1F1B. We will retrofit the formulation to adapt to VPP later. As for the communication time, it consists of the time of P2P communication in PP and collective communication in DP. It is modeled as the communication volume divided by the communication bandwidth. If the sizes of TP and DP are fixed, the communication time remains constant.

Constraints. Besides the objective function, we must consider constraints to ensure training feasibility. The first constraint is the resource constraint. The number of GPUs allocated to each module should be $x + y + z \leq N$ where N is the total number of GPUs in the cluster. The second constraint involves memory. We consider LLM backbone. Memory allocation involves four parts: model parameters, gradients, optimizer states, and activation states. The memory of model parameters and gradients on one GPU is calculated as: $\frac{P}{PP_{lm} \times TP_{lm}} = \frac{DP_{lm} \times P}{y}$, where P denotes total memory for the LLM parameters and gradients. The memory for optimizer states on one GPU (with ZeRO-1 optimization) is: $\frac{S}{y}$, where S denotes the total memory for the optimizer states. ZeRO-1 partitions the optimizer states across DP groups. The peak memory for activation states on one GPU is: $\frac{DP_{lm} \times L \times PP_{lm}}{y}$, with L representing the memory needed for one microbatch of activation states across the entire LLM. In 1F1B, the first PP stage requires storage for PP_{lm} microbatches of activation states. We eschew using GPipe in MMScale since GPipe consumes more memory. The memory constraint ensures the sum of the four memory parts on one GPU doesn't exceed GPU capacity. As for modality encoder and generator, the formulation is similar.

4.3 Adaptive Resource Allocation

The optimization problem is non-convex, with x, y, z , and the DP, TP sizes as positive variables. BS is predefined by the user. Solving this with an exhaust search algorithm to explore all possible variable values is impractical due to the extensive search space, particularly in large clusters. Designing an efficient algorithm that quickly identifies the optimal resource allocation and parallelism strategy is a significant challenge.

Convex optimization on resource allocation. Our key insight is to decompose the non-convex optimization problem into a series of simplified convex problems with variables x, y, z (i.e., the *resource allocation*). We confine the TP size to

Algorithm 1 Optimal adaptive resource allocation algorithm.

```

1: function RESOURCEALLOCATION
2:    $opt\_resource \leftarrow 0, opt\_parallelism \leftarrow 0, opt\_time \leftarrow +\infty$ 
3:   for parallelism in Possible_Parallelism_Set do
4:      $iter\_time, resource \leftarrow SLOVER(parallelism)$ 
5:     if  $iter\_time < opt\_time$  then
6:        $opt\_time \leftarrow iter\_time, opt\_resource \leftarrow resource$ 
7:      $opt\_parallelism \leftarrow parallelism$ 
8:   return  $opt\_resource, opt\_parallelism$ 

```

[1, 2, 4, 8] on an NVIDIA GPU node with 8 GPUs and adjust the DP size as a factor of BS to balance the computation across DP groups. The PP size of the LLM backbone is calculated as $\frac{y}{DP_{lm} \times TP_{lm}}$. The set of possible parallelism strategies is a manageable and finite set, i.e., the Cartesian product of the TP and DP size. This allows us to enumerate all feasible TP and DP sizes and transform the original optimization problem into a set of simplified problems. In the simplified problem, the objective function is maximal and additional of the functions: $\frac{1}{x}, \frac{1}{y}$ and $\frac{1}{z}$, where x, y, z are positive. Therefore, the objective function is convex. Similarly, the constraint functions are also convex. As a result, the simplified optimization problem is convex and can be efficiently solved to optimality by existing solvers [34, 35]. The algorithm, detailed in Algorithm 1, efficiently finds the optimal resource allocation and parallelism strategy to minimize iteration time.

Virtual pipeline parallelism (i.e., interleaved 1F1B) reduces the warm-up time by dividing model into finer-grained virtual PP (VPP) stages. Each PP stage contains VPP-size VPP stages. In the warm-up phase, each PP stage launches the computation of one VPP stage, and the warm-up time is divided by VPP-size. To align our formulation with VPP, we proportionally reduce the warm-up time based on VPP-size.

5 Addressing Data Heterogeneity

The data heterogeneity causes intra-microbatch and inter-microbatch stragglers. Addressing both straggler simultaneously renders the problem intractable due to its high complexity (e.g., the order of the training samples results in factorial-level complexity) and the necessity of runtime execution. To tackle this challenge, we decompose the overarching problem into two tractable subproblems. Initially, we present intra-microbatch reordering to eliminate stragglers across DP groups. We then introduce inter-microbatch reordering to minimize pipeline bubbles caused by the straggler microbatches. The combination of the two reordering, i.e., data-aware reordering, effectively addresses the data heterogeneity.

5.1 Intra-microbatch Reordering

Insight. To address the first subproblem of intra-microbatch stragglers, we identify the straggler by pinpointing the DP group with the largest training samples. As illustrated in Figure 6, the first DP group becomes a straggler as it contains the two largest training samples. To neutralize this imbalance, we propose reordering the training samples within the global

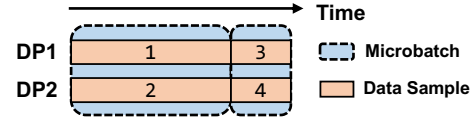


Figure 11: Intra-microbatch reordering.

batch by size. Specifically, as depicted in Figure 11, we reorder the training samples into the sequence [1, 3, 2, 4]. This strategy effectively distributes the computational load more evenly and improves the scalability. It eliminates the straggler without breaking the synchronous training semantics [31], as the reordering occurs within an individual global batch.

Intra-microbatch Reordering. Leveraging this insight, we propose intra-microbatch reordering to balance computational load and improve the overall scalability. Formally, the challenge involves minimizing the maximum computation time among DP groups. This problem corresponds to the NP-hard problem, multiway number partitioning [36], which aims to minimize the largest sum. There is no known polynomial-time algorithm capable of determining the optimal solution. Given the variability of runtime training samples, any algorithm employed must run before each iteration with negligible runtime overhead. Consequently, we adopt the greedy number partitioning algorithm, which guarantees an approximation ratio of $\leq \frac{4}{3}$ [37]. The detailed algorithm is summarized in Algorithm 2. The function *INTRAREORDER* receives the n original training samples and DP size m . This algorithm first sorts the training samples in ascending order by the sample size (line 3). Then, it loops over the training samples and assigns the sample to the DP group with the current lowest computational load (line 6-8). It then returns the reordered training samples (line 9-11). The algorithm is lightweight and maintains a time complexity of $O(n \log n + m \times n)$.

5.2 Inter-microbatch Reordering

The second subproblem is the inter-microbatch straggler. As we discussed in §2.3, data heterogeneity leads to varied computation times across microbatches within the modality encoder and generator. The straggler microbatch prolongs the training by creating large pipeline bubbles. In the context of 1F1B pipeline scheme, the overall iteration time is primarily governed by pipeline bubbles and the computation time at the first PP stage of the modality encoder, as illustrated in Figure 12. Let the PP size be p and the number of microbatches be l ($p = 4$ and $l = 6$ in Figure 12). Typically, l is larger than p to reduce the proportion of time spent in the warm-up and cool-down phases. We abstract an innovative concept, pipeline *intervals*, at the first PP stage. As shown in Figure 12, these intervals are typically filled with forward pass, except for the last $p - 1$ intervals (i.e., $interval_4, interval_5$, and $interval_6$). Straggler microbatches in either the encoder or generator prolong these intervals or increase the unfilled area (i.e., bubble). Designing an efficient runtime algorithm to minimize pipeline bubbles presents a significant challenge.

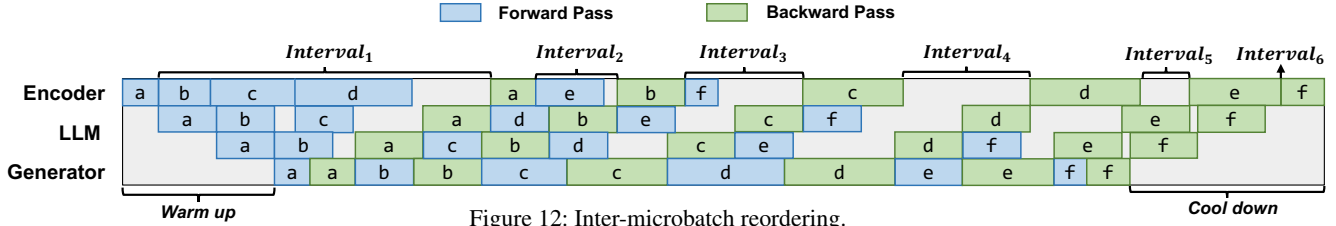


Figure 12: Inter-microbatch reordering.

Algorithm 2 Intra-batch reordering.

```

1: function INTRAREORDER( $\{d_1, \dots, d_n\}, m$ )
2:    $sorted\_samples \leftarrow \{d_1, \dots, d_n\}$ ,  $ret\_samples \leftarrow \emptyset$ ,  $Groups \leftarrow \emptyset$ 
3:   Sort  $sorted\_samples$  in ascending order based on  $d_i.size$ 
4:   for  $i = 1 \rightarrow m$  do
5:      $Group_i \leftarrow \emptyset$ ,  $Groups.append(Group_i)$ 
6:   for  $i = 1 \rightarrow n$  do
7:      $min\_index \leftarrow argmin_j \sum_{d \in Group_j} d.size$ 
8:      $Groups[min\_index].append(sorted\_samples[i])$ 
9:   for  $i = 1 \rightarrow m$  do
10:     $ret\_samples.append(Groups[i])$ 
11:   return  $ret\_samples$ 

```

Insights. We leverage two insights to solve this problem. The first insight involves minimizing the volume of intervals that cannot be filled. As shown in Figure 12, the last $p - 1$ intervals (i.e., $interval_{l-p+2}$ to $interval_l$) remain unfilled. These intervals become the pipeline bubbles and prolong the training iteration. We observe a positive correlation between the volume of $interval_i$ and the size of the i_{th} microbatch. For instance, $interval_4$ is significantly larger than $interval_5$ and $interval_6$. By strategically reordering the training samples to position the smallest $p - 1$ microbatches at the end, we are able to reduce these unfilled intervals (i.e., pipeline bubbles).

The second insight involves minimizing the unfilled area of front intervals. As shown in Figure 12, the first interval is filled with by the 2_{nd} to p_{th} microbatches' forward passes. The volume of the first interval (i.e., $bubble_a$) is determined by the aggregate forward and backward times of the first microbatch in LLM backbone and modality generator. Such characteristic allows the accommodation of large microbatches early in the sequence to fill the first interval. For subsequent intervals, $interval_i$ is filled by the $(i + p - 1)_{th}$ microbatch's forward pass. By evaluating the volume of $interval_i$, we place the microbatch, whose forward time most closely matches this volume, at the $(i + p - 1)_{th}$ position, thereby reducing the unfilled area (i.e., pipeline bubbles).

Inter-microbatch Reordering. Based on the two insights, we design runtime inter-microbatch reordering to minimize the pipeline bubbles. This algorithm is designed for 1F1B pipeline scheme. We will retrofit the algorithm to VPP (i.e., interleaved 1F1B) later. Algorithm 3 summarizes the pseudo code. The function *INTERREORDER* receives the original order of microbatches and the PP size p . It stores reordered microbatches in ret_mb and pending microbatches in mb (line 2). Early in the process, the smallest microbatch is placed at first

Algorithm 3 Inter-batch reordering.

```

1: function INTERREORDER( $\{m_1, \dots, m_l\}, p$ )
2:    $ret\_mb \leftarrow \emptyset$ ,  $mb \leftarrow \{m_1, \dots, m_l\}$ 
3:    $ret\_mb.append(MIN(mb))$ ,  $mb.remove(MIN(mb))$ 
4:    $rear\_mb \leftarrow SELECTMIN(mb, p - 1)$ ,  $mb.remove(rear\_mb)$ 
5:   for  $i = 1 \rightarrow l - p$  do
6:      $interval_i \leftarrow GETINTERVAL(ret\_mb, i)$ 
7:     if  $i == 1$  then
8:        $cur\_mb \leftarrow SELECTCLOSEST(mb, p - 1, interval_i)$ 
9:     else
10:       $cur\_mb \leftarrow SELECTCLOSEST(mb, 1, interval_i)$ 
11:    $ret\_mb.extend(cur\_mb)$ ,  $mb.remove(cur\_mb)$ 
12:    $ret\_mb.extend(rear\_mb)$ 
13:   return  $ret\_mb$ 

```

to activate all pipeline stages promptly (line 3). Subsequently, it selects the smallest $p - 1$ microbatches and places them at the end to minimize unfilled intervals (line 4 and line 12). It then loops over the remaining microbatches (line 5-11). In each loop iteration, it calculates the volume of the interval through the function *GETINTERVAL*. For the first interval, it selects $p - 1$ microbatches that closely match the interval volume in sum forward time; for others, it selects a single microbatch whose forward time aligns closely with the interval volume. This loop ensures maximal filling of the remaining intervals, which minimizes pipeline bubbles.

The functions *SELECTMIN* and *SELECTCLOSEST* operate with a time complexity of $O(l)$. The function *GETINTERVAL* calculates interval volumes using the current order ret_mb . This calculation is facilitated by a dynamic programming algorithm that utilizes a recursive formula derived from pipeline dependencies. Specifically, each microbatch's start time depends on two factors: the completion of the preceding microbatch on the same device and the availability of input data from the upstream microbatch. Consequently, the end time of each microbatch is determined by the maximum of these two dependencies plus its own computation time. This dynamic programming algorithm exhibits a complexity of $O(p)$ per function invocation. The algorithm is lightweight and efficient with a time complexity of $O(l \times (l + p))$.

Virtual pipeline parallelism (i.e., interleaved 1F1B) also follows the one forward and one backward pipeline scheme to reduce the memory footprint. The fundamental insights of our algorithm apply universally to any 1F1B-based pipeline, including VPP. We adapt the algorithm by computing multiple (i.e., VPP size) intervals and filling them with the corresponding number of forward passes from a single microbatch.

6 System Implementation and Optimization

We implement MMScale with 6.3K lines of code in Python and C++, and integrate it with Megatron-LM [17], a state-of-the-art training framework for large language models. MMScale is able to support multimodal LLM training with a variety of modalities on a large-scale GPU cluster (e.g., thousands of GPUs used in §7). MMScale leverages a distributed file system to store the training data and model checkpoints. It handles failures by automatically recovering the training process from the latest checkpoint.

MMScale orchestrator. MMScale’s training orchestrator, implemented as a Python script on a dedicated CPU node, formulates the adaptive resource allocation problem using Disciplined Convex Programming [38]. It employs the CVX solver [39] to efficiently solve this problem within milliseconds. The orchestrator then records the optimal resource allocation and parallelism strategy to a configuration file, which the Kubernetes controller uses to launch the training task.

MMScale initializer. MMScale incorporates parallelism unit that manages specific parallelism strategies for each module in multimodal LLMs. Parallelism unit is initialized using PyTorch Distributed [40] library with NCCL as the default communication backend, except for the TP communication where we use StepCCL instead. MMScale shards the model parameters in accordance with the established parallelism strategy.

Parallelism unit. As we discussed in §4.1, the disaggregated training is implemented through a specific module: *parallelism unit*. When initializing the distributed training, MMScale first establishes the communication groups within one parallelism unit. Each GPU process has a global rank and a local rank within the unit, which facilitates the distributed initialization. Then, it initializes the communication broker to establish the PP communication between adjacent parallelism units. All communication traffic between parallelism units is routed via the communication broker.

We implement the communication broker by modifying the batched send and receive operations in Megatron-LM to separate operations. This allows flexible communication between multiple upstream and downstream GPU processes. The communication broker adjusts the communication data by concentrating and scattering the data as needed while maintaining the data order. Strategically located on the GPU of the last PP stage in the upstream unit or the first PP stage in the downstream unit, the communication broker avoids additional communication overhead. Besides, the number of communication brokers between two units is determined by the greatest common divisor of the two parallelism units’ DP sizes to maximize the communication bandwidth. Moreover, in the Megatron-LM, the reliance on synchronous communication compels upstream stages to pause until downstream stages fully receive the data. This introduces unnecessary de-

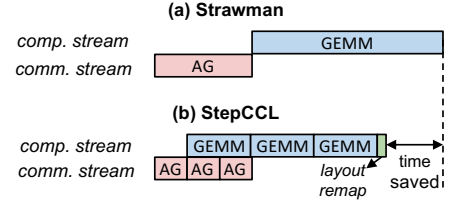


Figure 13: Overlapping communication and computation.

pendencies in the pipeline. To alleviate this, we implement asynchronous send operations that eliminate these superfluous dependencies and redesign the communication topology to prevent potential deadlocks.

Asynchronous data loader. When training multimodal LLMs, training samples often combine lightweight text with heavyweight multimodal data. The latter significantly increases data loading time. For example, a typical training sample could include a 256-word text sequence and ten 1024×1024 RGB images. The text is just kilobytes, whereas the images are total of 120 megabytes. Loading multiple such samples can take several seconds. MMScale’s data loader employs a producer-consumer model to enhance efficiency. The producer, operating on dedicated CPU nodes, fetches data from the distributed file system and pre-processes training data (e.g., image cropping) asynchronously with the GPU training process. The consumer, integrated within the main training process, receives this pre-processed data and reorders it to eliminate the data heterogeneity. The producer and consumer communicate through RPC calls, and use RDMA network for lower latency if available.

Mitigating TP overhead with StepCCL. Tensor Parallelism (TP) is commonly adopted to facilitate training large Transformer-based models with multiple GPUs connected with high bandwidth (e.g., with NVLinks). Specifically, TP divides the linear layers, into smaller sub-modules, which are then distributed across the GPUs. After parallel computation, all GPUs perform collective communication to aggregate data and produce identical results. The TP communication overhead severely degrades overall performance, especially on A800 and H800 GPUs with restricted NVLink bandwidth.

We implement the communication overlap with an in-house collective communication library called StepCCL to reduce the TP overhead. StepCCL is a PyTorch custom plugin that performs cross-GPU collective communication, including allgather, reduce-scatter, and allreduce, which is similar to NCCL. However, NCCL occupies several CUDA Streaming Multiprocessors (SMs) for executing its communication kernel and is known to harm the performance of its concurrent GEMM (matrix multiplication) [41]. To solve this, StepCCL leverages the DMA engine directly to perform data transmission without using any SM at all. This enables StepCCL and GEMM to run simultaneously on a GPU without slowing down each other. This cornerstone facilitates our subsequent development of communication overlap.

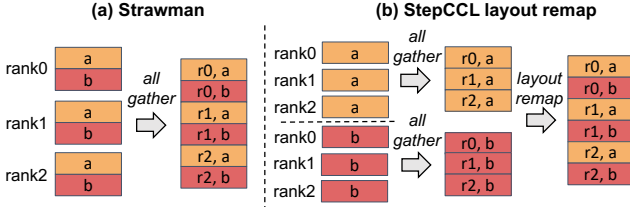


Figure 14: Layout remap.

Figure 13 shows an example of how StepCCL works in overlapping the allgather (AG) operation with GEMM. We start by decomposing the single GEMM and the corresponding communication into several smaller pairs. Each small communication operation starts sequentially on a communication stream, with its paired GEMM executed on the default computation stream. The communication overhead is fully hidden except for the first allgather.¹ After all GEMMs finish, we perform an extra layout remapping operation (usually with negligible overhead) to ensure identical results with the baseline. Figure 14 describes the details of the layout remap process. In some rare cases during backward propagation, we find the remap overhead is high due to certain model dimension. To mitigate this, we further overlap the remap with the computation of the weight gradients, so eventually we nearly get the full performance gain of the communication overlap.

Finally, although the overlap idea is also studied in many related works [42–44], we highlight the key differences of ours. Unlike prior work that fuses GEMM with TP communication into one CUDA kernel [42, 43], we choose a modular design and do not use fusion for more flexibility. For example, when TP communication is longer than GEMM, fusing them cannot fully hide the communication overhead. However, with the modular design, we are able to hide the communication with other modules without dependency (e.g., in cross-attention), which is not possible with the fused implementation. This enables broader adoption of StepCCL in many other scenarios.

7 Evaluation

In this section, we first use large-scale experiments to demonstrate the overall performance improvements of MMScale over existing multimodal LLM training solution. Next, we use microbenchmarks to deep dive into MMScale and show the effectiveness of each component of MMScale. Finally, we conduct a case study to evaluate MMScale under different frozen settings and evaluate the system optimizations.

Setup. Our experiments are conducted on a production GPU cluster for multimodal LLM training, with each node equipped with eight NVIDIA A800 GPUs, 1TB of memory, and 96 vCPUs. GPUs within one node are interconnected by 300GB/s

¹If the number of allgather/GEMM is large enough, the only allgather in the critical path should have negligible overhead. But dividing a large GEMM into finer granularity sometimes could lead to overall slowdown. In practice, the number is actually configurable.

Models	# of Layers	Hidden Size	FFN Hidden Size	# of Heads	# of Groups
Llama3-7B	32	4096	11008	32	32
Llama3-13B	40	5120	13824	40	40
Llama3-70B	80	8192	28672	64	8

Table 1: LLM backbone configurations.

(bidirectional) NVLink, while nodes are connected by 4*200 Gbps RDMA network based on RoCEv2 with rail-optimized topology. The overall experiments use up to 1296 GPUs, and the microbenchmark utilizes up to 98 GPUs. We use PyTorch 2.1.2 and NVIDIA CUDA 12.2 for our evaluation.

Models. For LLM backbone, we choose the representative LLM architecture, Llama3 [22], which is widely used in both academia and industry. Table 1 lists the detailed model configurations. As for the modality, we focus on images and texts. MMScale is also compatible with other modalities. For modality encoder and modality generator, we use ViT-Huge [45] (0.63B) and Stable-Diffusion 2.1 [46] (1B) respectively. These two models are widely used for image understanding and generation. The three LLM backbones (i.e., Llama3-7B, Llama3-13B, and Llama3-70B) are paired with ViT-Huge and Stable-Diffusion to form multimodal LLMs designated as MLLM-9B, MLLM-15B, and MLLM-72B. For large multimodal LLM (i.e., MLLM-72B), we use high image resolution (i.e., 1024×1024) for generation since the large LLM is able to process more context information. For small models, we use low image resolution (i.e., 512×512).

Datasets. For our experiments, we use the representative open-source dataset, LAION-400M. We generate training data by interleaving the image and text subsequences, forming input sequences up to 8192 tokens long. This dataset is also employed in our production multimodal LLM training. As detailed in §2.3, each training sample includes a varying number of image tokens and text tokens, which introduces data heterogeneity in multimodal LLM training.

Metrics. We use the Model FLOPs Utilization (MFU) as the primary metric to evaluate MMScale. MFU measures the percentage of GPU FLOPs that are effectively utilized during model training. We also use the training throughput (TPT.) to evaluate the training speed of MMScale. Since MMScale and Megatron-LM may utilize different numbers of GPUs due to varying resource allocation strategies, we also indicate the number of GPUs used in the throughput charts.

7.1 Overall Performance

Setup. We first compare the overall performance of MMScale against Megatron-LM on a large-scale GPU cluster (up to 1296 GPUs). We retrofit Megatron-LM to support multimodal LLM training by integrating modality encoder and generator into the training pipeline. Megatron-LM employs rigid resource allocation as described in §2.1. In Megatron-LM, we set the PP size of the LLM backbone to 1, 2, and 10 for

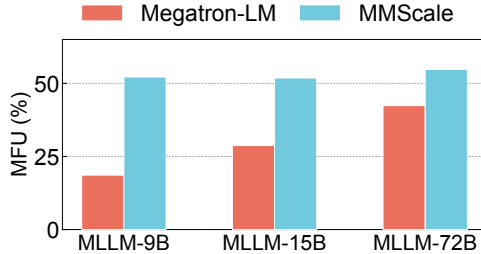


Figure 15: The overall MFU of MMScale and Megatron-LM.

Llama3-7B, Llama3-13B, and Llama3-70B, respectively. TP size is set to 8. As for MMScale, the parallelism strategy is determined by adaptive resource allocation. In our experiments, one GPU is able to facilitate training ViT and Stable-Diffusion. For both Megatron-LM and MMScale, we replicate the encoder and generator across the GPUs within the TP group to process different image subsequences, whereas TP itself is not used. We set global batch size to 1920.

The experimental results are shown in Figure 15 and Figure 16. Figure 15 shows the MFU of MMScale and Megatron-LM under different multimodal LLMs. Figure 16 shows the training throughput and marks the number of GPUs used in each experiment. We summarize the experiment as follows.

- As shown in Figure 15, MMScale achieves 51.8%-54.7% MFU under large-scale multimodal LLM training scenario. This performance closely approximates that of state-of-the-art unimodal (i.e., text) LLM training [29], which demonstrates the effectiveness of MMScale in eliminating the model and data heterogeneity in multimodal LLM training.
- MMScale significantly outperforms Megatron-LM, delivering 1.7-2.8 \times the MFU and 1.7-2.2 \times the training throughput when training MLLM-9B and MLLM-15B with a similar number of GPUs. These performance gains largely stem from MMScale’s adaptive resource allocation strategy. Megatron-LM’s rigid strategy often leads to GPU underutilization in multimodal modules, since it assigns too many GPUs to the modality encoder and generator. In contrast, MMScale adaptively adjusts GPU allocations based on specific model and data demands. Additionally, MMScale’s data-aware reordering technique further boosts efficiency.
- In MLLM-72B training scenario, MMScale also outperforms Megatron-LM by 1.2 \times on MFU and 1.3 \times on training throughput with a similar number of GPUs. The high image resolution prolongs the execution time of the multimodal module, which introduces pipeline bubbles in LLM backbone. MMScale addresses this by allocating additional GPUs to these modules to balance the pipeline. MMScale’s data-aware reordering strategy continues to diminish data heterogeneity, thereby increasing overall training efficiency.

7.2 Deep Dive into MMScale

In this subsection, we perform microbenchmarks to evaluate the effectiveness of each MMScale’s component. Our experiments utilize up to 98 NVIDIA A800 GPUs. We set the global

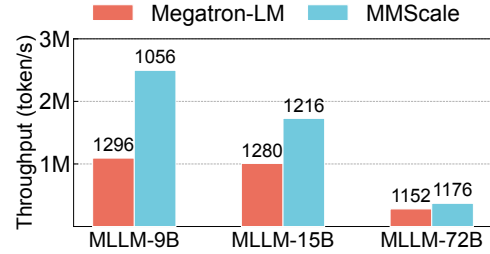


Figure 16: The overall throughput of MMScale and Megatron-LM.

batch size to 128, 64, and 40 for MLLM-9B, MLLM-15B, and MLLM-72B, respectively.

7.2.1 Adaptive Resource Allocation

We measure the MFU and training throughput of MMScale and other resource allocation strategies, including a comparison with Megatron-LM and a ratio-based approach. The ratio-based strategy allocates GPUs according to the computational demands (flops) of each module. We also annotate the total number of GPUs utilized in the throughput chart. The experimental results are shown in Figure 17. MMScale consistently outperforms the baseline strategies, achieving 1.3%-2.7% higher MFU and 1.4%-2.7% higher training throughput. Although the ratio-based strategy outperforms Megatron-LM’s rigid allocation, it still lags behind MMScale since it neglects the intricate performance model (§4.2) of multimodal LLM training. MMScale employs an adaptive resource allocation strategy that optimally balances computational loads across the three modules and achieves high resource utilization.

We also evaluate the running time of MMScale’s resource allocation algorithm under different training settings, as detailed in Table 2. The algorithm completes the allocation process in under one second. The overhead is negligible compared to the days or even weeks required for overall training.

7.2.2 Data-aware Reordering

We evaluate the effectiveness of MMScale’s data-aware reordering by comparing it against the random order set by PyTorch’s DataLoader, while keeping other components the same. The effectiveness is gauged through metrics such as MFU and training throughput (TPT.). We use the optimal resource allocation and parallelism strategy decided by MMScale’s adaptive resource allocation algorithm. Given that the GPU allocation policy remains unchanged, the number of GPUs is not specified in this experiment. The experimental settings are the same as those in §7.2.1. The results are shown in Figure 18. MMScale consistently outperforms the baseline, achieving 1.03%-1.11% higher MFU and training throughput. The performance gap becomes more pronounced as the model size decreases. This is because the smaller model size leads to a higher data parallelism (DP) size, which causes more inter-microbatch heterogeneity. In essence, MMScale’s data-aware reordering effectively mitigates data heterogeneity and enhances the training efficiency.

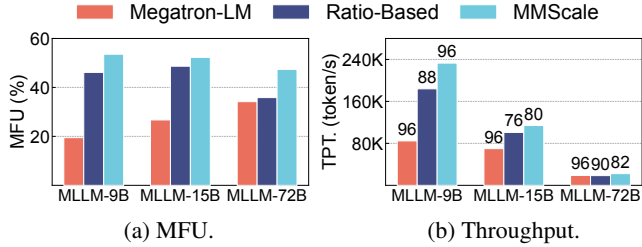


Figure 17: Effectiveness of sysname’s adaptive resource allocation.

Model	# of GPUs	Global Batch Size	Algorithm Overhead
MLLM-72B	1296	1920	922ms
MLLM-72B	648	960	641ms
MLLM-72B	324	480	441ms
MLLM-72B	112	240	133ms

Table 2: Algorithm overhead of adaptive resource allocation.

MMScale’s data-aware reordering algorithm executes before each training iteration. Table 3 presents a detailed analysis of the runtime overhead of the reordering algorithm. The DP size is the number of data parallelism groups in modality encoder. It completes the reordering in just a few milliseconds, a duration that is negligible compared to the several seconds to tens of seconds required for one iteration.

7.3 Case Study

In this subsection, we first evaluate MMScale under different frozen training settings. We then evaluate the effectiveness of system optimizations tailored for multimodal LLM training.

7.3.1 Frozen Training

We conduct a frozen training experiment under four specific training settings: complete module freezing, exclusive encoder training, exclusive LLM training, and exclusive generator training. We keep training the projectors. In these scenarios, frozen modules neither compute weight gradients nor update weights. All other experimental setup aligns with those detailed in §7.2. We evaluate the MFU and training throughput (TPT.) of MMScale compared to Megatron-LM. The experimental results are presented in Figure 19 and Figure 20. MMScale consistently outperforms Megatron-LM across all frozen training configurations, achieving 1.4%-2.9% higher MFU and 1.2%-2.9% increased training throughput. This pronounced performance gap underscores the challenges posed by Megatron-LM’s rigid resource allocation in complex training environments. In contrast, MMScale adaptively adjusts resource allocation based on training settings and consistently achieves high resource utilization.

7.3.2 System Optimizations

Asynchronous Data Loader. We conduct an experiment to evaluate the effectiveness of asynchronous data loading optimization. Setting the DP size to one, we measure the average data loading time per iteration solely on the CPU. We then

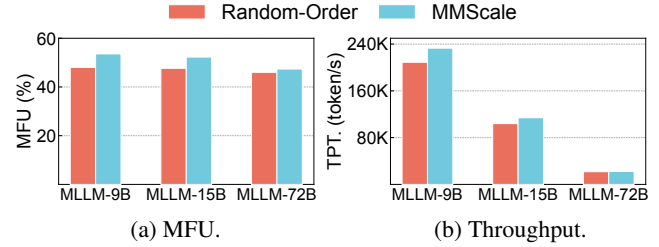


Figure 18: Effectiveness of MMScale’s data-aware reordering.

Model	DP Size	Global Batch Size	Intra-microbatch Reordering	Inter-microbatch Reordering
MLLM-72B	30	1920	1.82ms	5.87ms
MLLM-72B	60	1920	1.87ms	3.02ms
MLLM-72B	120	1920	1.89ms	1.71ms

Table 3: Algorithm overhead of data-aware reordering.

compare data loading times with and without this optimization and use varying numbers of images and different image resolutions for one training iteration. The results, depicted in Figure 21, indicate that asynchronous data loading significantly reduces loading time from seconds to milliseconds. The first parameter in the x-axis represents the number of images, while the second parameter denotes the image resolution. This reduction renders the loading time negligible relative to the total training time.

Mitigating TP overhead with StepCCL. To evaluate the effectiveness of StepCCL in mitigating the TP overhead, we conduct an experiment that measures the iteration time of the LLM backbone with training of one single PP stage (i.e., one minimal TP group) under various TP sizes. We compare the iteration time with and without StepCCL enabled. The results are shown in Figure 22. StepCCL significantly reduces the iteration time by overlapping the TP communication with computation. It outperforms the baseline by 1.1-1.17 \times when the TP size is 4 and 1.15-1.17 \times when the TP size is 8. The gains are more pronounced at large TP size, where communication overhead is more substantial. These findings confirm that StepCCL effectively mitigates TP overhead.

8 Discussion

Parallelism optimization. Many studies [47–49] refine parallelism strategies for deep learning models, but they fall short for multimodal LLMs due to their expansive search spaces and large cluster requirements. These methods separately optimize different strategies, resulting in inefficient parallelism. Additionally, these methods generally assume data homogeneity, standardizing computations across all training samples. This assumption does not hold for multimodal LLMs due to the data heterogeneity in modality inputs of each sample. In contrast, MMScale leverages the specific training pattern of multimodal LLMs, creating a customized resource allocation problem that integrates tensor, pipeline, and data parallelism

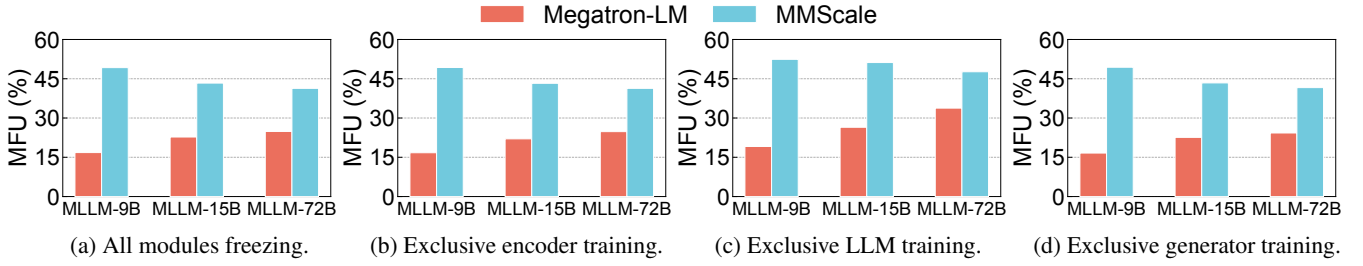


Figure 19: MFU under frozen training setting.

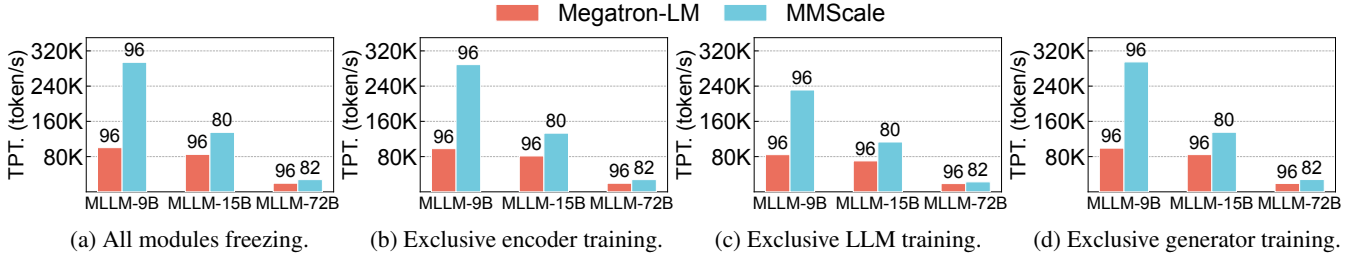


Figure 20: Throughput under frozen training setting.

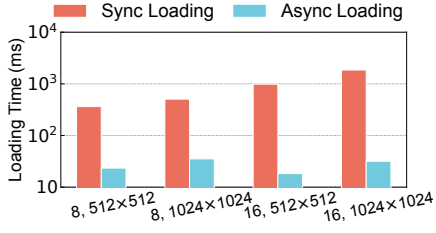


Figure 21: Asynchronous data loading.

simultaneously. Besides, MMScale leverages data-aware re-ordering to harness the data heterogeneity.

Sequence and expert parallelism. Sequence parallelism (SP) [50] is designed to partition the training sequence into multiple subsequences for parallel training. It addresses the challenges of processing long sequences in LLMs. Expert parallelism (EP) [51], specifically devised for mixture-of-experts (MoE) LLMs [52], enables parallel training of multiple feed-forward network (FFN) experts. These parallelism strategies are orthogonal to multimodal LLM training. In MMScale, both SP and EP are integrated into the training framework. MMScale treats SP and EP sizes as predefined parameters in the adaptive resource allocation optimization problem.

Disaggregating multimodal modules from LLM. In MMScale, we address model heterogeneity by treating multimodal modules and LLM as separate stages in pipeline parallelism (PP). Another approach might integrate some LLM layers with multimodal modules into the same PP stage, while distributing the remaining LLM layers to maintain balance. However, this often becomes suboptimal since it requires multimodal modules to adopt the same TP strategy as the LLM layers within the same PP stage. Such alignment degrades performance when the optimal TP strategies for multimodal modules differ from those of LLM layers. Therefore, we choose

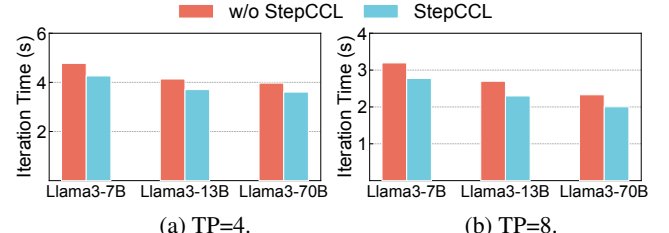


Figure 22: Overlapping the TP communication with computation.
to disaggregate multimodal modules from LLM as separate PP stages to achieve better performance.

9 Related Work

LLM training. Many efforts have been made to optimize the training of LLMs from system perspectives. For LLM pretrain, Megatron-LM [17] and DeepSpeed-Megatron [53] propose customized 3D-parallelism and are de facto standards for training large LLMs. DeepSpeed-ZeRO [32] and Pytorch-FSDP [54] reduce redundant memory consumption in data parallelism. HPN [55] proposes a new dual-ToR network architecture trailed for LLM training to reduce ECMP conflict. A set of works [29, 42–44, 56] overlap the communication and computation operators in LLM training. Fault tolerance through replication and checkpoint is advanced in large training clusters by studies [29, 57]. Efforts like [58–60] further optimize recovery process in cloud spot instance scenarios. These system optimizations of LLM training are orthogonal to MMScale. They overlook the model and data heterogeneity in multimodal LLMs. MMScale also integrates several of these optimizations in training the LLM backbone.

Multimodal model training. Small multimodal models (e.g., CLIP [61] and LiT [62]) have been widely studied in recent years. Many system optimizations have been proposed to train such multimodal models efficiently. DistMM [63]

tackles model heterogeneity by introducing modality-aware placement and partitioning to evenly distribute workload. GraphPipe [64] presents graph pipeline parallelism, addressing graph dependencies in multimodal models to minimize pipeline bubbles. Yet, these advancements primarily enhance small multimodal models trained on tens of GPUs. They fall short for scaling up to meet the demands of integrating multimodal models with LLMs which necessitate training across thousands of GPUs. This gap underpins the motivation behind MMScale, designed to meet the unique challenges of multimodal large language model training.

Multimodal LLM serving. LLM serving has been widely studied in recent years. Orca [65], FastServe [66], and VTC [67] propose iteration-level scheduling algorithms to improve the serving quality. DistServe [68] and Splitwise [69] propose disaggregated serving for prefill and decoding to improve the serving throughput. vLLM [70], RAGCache [71], and SGLang [72] propose prefix caching to reuse the KV tensors. However, the serving of multimodal LLMs remains under-explored. MMScale’s core insights (e.g., disaggregated modules) are applicable to multimodal LLMs serving. Our future work will delve into the specific challenges posed by multimodal LLMs serving systems.

10 Conclusion

We present MMScale, an efficient and adaptive framework to reform the training of multimodal LLMs. We identify the key challenges in training multimodal LLMs, i.e., model heterogeneity and data heterogeneity. MMScale introduces novel adaptive resource allocation to eliminate model heterogeneity and data-aware reordering to mitigate data heterogeneity. We evaluate MMScale on production cluster with thousands of GPUs and show that it achieves 54.7% MFU and outperforms Megatron-LM by up to 2.2 \times on throughput.

References

- [1] “Introducing chatgpt.” <https://openai.com/blog/chatgpt>, 2022.
- [2] H. Liu, W. Yan, M. Zaharia, and P. Abbeel, “World model on million-length video and language with block-wise ringattention,” *arXiv preprint arXiv:2402.08268*, 2024.
- [3] P. Zhang, X. D. B. Wang, Y. Cao, C. Xu, L. Ouyang, Z. Zhao, S. Ding, S. Zhang, H. Duan, H. Yan, *et al.*, “Internlm-xcomposer: A vision-language large model for advanced text-image comprehension and composition,” *arXiv preprint arXiv:2309.15112*, 2023.
- [4] W. Wang, Z. Chen, X. Chen, J. Wu, X. Zhu, G. Zeng, P. Luo, T. Lu, J. Zhou, Y. Qiao, *et al.*, “Visionllm: Large language model is also an open-ended decoder for vision-centric tasks,” in *Advances in Neural Information Processing Systems*, 2024.
- [5] D. Zhu, J. Chen, X. Shen, X. Li, and M. Elhoseiny, “Minigpt-4: Enhancing vision-language understanding with advanced large language models,” *arXiv preprint arXiv:2304.10592*, 2023.
- [6] P. K. Rubenstein, C. Asawaroengchai, D. D. Nguyen, A. Bapna, Z. Borsos, F. d. C. Quiry, P. Chen, D. E. Badawy, W. Han, E. Kharitonov, *et al.*, “Audiopalm: A large language model that can speak and listen,” *arXiv preprint arXiv:2306.12925*, 2023.
- [7] Z. Borsos, R. Marinier, D. Vincent, E. Kharitonov, O. Pietquin, M. Sharifi, D. Roblek, O. Teboul, D. Grangier, M. Tagliasacchi, *et al.*, “Audiolm: a language modeling approach to audio generation,” *IEEE/ACM transactions on audio, speech, and language processing*, 2023.
- [8] C. Zhang, J. Chen, J. Li, Y. Peng, and Z. Mao, “Large language models for human-robot interaction: A review,” *Biomimetic Intelligence and Robotics*, 2023.
- [9] D. Driess, F. Xia, M. S. Sajjadi, C. Lynch, A. Chowdhery, B. Ichter, A. Wahid, J. Tompson, Q. Vuong, T. Yu, *et al.*, “Palm-e: An embodied multimodal language model,” *arXiv preprint arXiv:2303.03378*, 2023.
- [10] “Hello gpt-4o.” <https://openai.com/index/hello-gpt-4o/>, 2024.
- [11] “Introducing gemini: our largest and most capable ai model.” <https://blog.google/technology/ai/google-gemini-ai/>, 2024.
- [12] C. Team, “Chameleon: Mixed-modal early-fusion foundation models,” *arXiv preprint arXiv:2405.09818*, 2024.
- [13] J. Kaplan, S. McCandlish, T. Henighan, T. B. Brown, B. Chess, R. Child, S. Gray, A. Radford, J. Wu, and D. Amodei, “Scaling laws for neural language models,” *arXiv preprint arXiv:2001.08361*, 2020.
- [14] “Openai’s gpt-3 language model: A technical overview.” <https://lambdalabs.com/blog/demystifying-gpt-3>, 2020.
- [15] S. Yin, C. Fu, S. Zhao, K. Li, X. Sun, T. Xu, and E. Chen, “A survey on multimodal large language models,” *arXiv preprint arXiv:2306.13549*, 2023.
- [16] D. Zhang, Y. Yu, C. Li, J. Dong, D. Su, C. Chu, and D. Yu, “Mm-lmms: Recent advances in multimodal large language models,” *arXiv preprint arXiv:2401.13601*, 2024.
- [17] M. Shoeybi, M. Patwary, R. Puri, P. LeGresley, J. Casper, and B. Catanzaro, “Megatron-lm: Training multi-billion parameter language models using model parallelism,” *arXiv preprint arXiv:1909.08053*, 2019.

[18] A. Vaswani, N. Shazeer, N. Parmar, J. Uszkoreit, L. Jones, A. N. Gomez, Ł. Kaiser, and I. Polosukhin, “Attention is all you need,” in *Advances in Neural Information Processing Systems*, 2017.

[19] A. Radford, J. Wu, R. Child, D. Luan, D. Amodei, I. Sutskever, *et al.*, “Language models are unsupervised multitask learners,” *OpenAI blog*, 2019.

[20] T. Brown, B. Mann, N. Ryder, M. Subbiah, J. D. Kaplan, P. Dhariwal, A. Neelakantan, P. Shyam, G. Sastry, A. Askell, *et al.*, “Language models are few-shot learners,” in *Advances in Neural Information Processing Systems*, 2020.

[21] J. Achiam, S. Adler, S. Agarwal, L. Ahmad, I. Akkaya, F. L. Aleman, D. Almeida, J. Altenschmidt, S. Altman, S. Anadkat, *et al.*, “Gpt-4 technical report,” *arXiv preprint arXiv:2303.08774*, 2023.

[22] “Meta llama3.” <https://llama.meta.com/>, 2024.

[23] P. Villalobos, A. Ho, J. Sevilla, T. Besiroglu, L. Heim, and M. Hobbhahn, “Position: Will we run out of data? limits of llm scaling based on human-generated data,” in *Forty-first International Conference on Machine Learning*.

[24] J.-B. Alayrac, J. Donahue, P. Luc, A. Miech, I. Barr, Y. Hasson, K. Lenc, A. Mensch, K. Millican, M. Reynolds, *et al.*, “Flamingo: a visual language model for few-shot learning,” in *Advances in Neural Information Processing Systems*, 2022.

[25] A. Dosovitskiy, L. Beyer, A. Kolesnikov, D. Weissenborn, X. Zhai, T. Unterthiner, M. Dehghani, M. Minnderer, G. Heigold, S. Gelly, *et al.*, “An image is worth 16x16 words: Transformers for image recognition at scale,” *arXiv preprint arXiv:2010.11929*, 2020.

[26] S. Chen, Y. Wu, C. Wang, S. Liu, D. Tompkins, Z. Chen, and F. Wei, “Beats: Audio pre-training with acoustic tokenizers,” *arXiv preprint arXiv:2212.09058*, 2022.

[27] R. Rombach, A. Blattmann, D. Lorenz, P. Esser, and B. Ommer, “High-resolution image synthesis with latent diffusion models,” in *IEEE Conference on Computer Vision and Pattern Recognition*, 2022.

[28] H. Liu, Z. Chen, Y. Yuan, X. Mei, X. Liu, D. Mandic, W. Wang, and M. D. Plumbley, “Audiodlm: Text-to-audio generation with latent diffusion models,” *arXiv preprint arXiv:2301.12503*, 2023.

[29] Z. Jiang, H. Lin, Y. Zhong, Q. Huang, Y. Chen, Z. Zhang, Y. Peng, X. Li, C. Xie, S. Nong, *et al.*, “Megascale: Scaling large language model training to more than 10,000 gpus,” in *USENIX NSDI*, 2024.

[30] C. Schuhmann, R. Vencu, R. Beaumont, R. Kaczmarczyk, C. Mullis, A. Katta, T. Coombes, J. Jitsev, and A. Komatsuzaki, “Laion-400m: Open dataset of clip-filtered 400 million image-text pairs,” *arXiv preprint arXiv:2111.02114*, 2021.

[31] “Techniques and systems to train and serve bigger models.” <https://icml.cc/virtual/2022/tutorial/18440>, 2022.

[32] S. Rajbhandari, J. Rasley, O. Ruwase, and Y. He, “Zero: Memory optimizations toward training trillion parameter models,” in *International Conference for High Performance Computing, Networking, Storage and Analysis*, 2020.

[33] P. Micikevicius, S. Narang, J. Alben, G. Diamos, E. Elsen, D. Garcia, B. Ginsburg, M. Houston, O. Kuchaiev, G. Venkatesh, *et al.*, “Mixed precision training,” *arXiv preprint arXiv:1710.03740*, 2017.

[34] M. Grant and S. Boyd, “Cvx: Matlab software for disciplined convex programming, version 2.1,” 2014.

[35] P. Virtanen, R. Gommers, T. E. Oliphant, M. Haberland, T. Reddy, D. Cournapeau, E. Burovski, P. Peterson, W. Weckesser, J. Bright, *et al.*, “Scipy 1.0: fundamental algorithms for scientific computing in python,” *Nature methods*, 2020.

[36] R. E. Korf, “Multi-way number partitioning,” in *Twenty-first international joint conference on artificial intelligence*, 2009.

[37] S. Barman and S. K. Krishnamurthy, “Approximation algorithms for maximin fair division,” *ACM Transactions on Economics and Computation (TEAC)*, 2020.

[38] M. Grant, S. Boyd, and Y. Ye, *Disciplined convex programming*. 2006.

[39] “Cvxpy 1.5.” <https://www.cvxpy.org/>, 2024.

[40] “Pytorch distributed overview.” https://pytorch.org/tutorials/beginner/dist_overview.html, 2024.

[41] S. Rashidi, M. Denton, S. Sridharan, S. Srinivasan, A. Suresh, J. Nie, and T. Krishna, “Enabling Compute-Communication Overlap in Distributed Deep Learning Training Platforms,” in *ACM/IEEE ISCA*, 2021.

[42] L.-W. Chang, W. Bao, Q. Hou, C. Jiang, N. Zheng, Y. Zhong, X. Zhang, Z. Song, Z. Jiang, H. Lin, X. Jin, and X. Liu, “FLUX: Fast Software-based Communication Overlap On GPUs Through Kernel Fusion,” 2024.

[43] “NVIDIA Transformer Engine,” 2024. <https://github.com/NVIDIA/TransformerEngine>.

[44] S. Wang, J. Wei, A. Sabne, A. Davis, B. Ilbeyi, B. Hechtman, D. Chen, K. S. Murthy, M. Maggioni, Q. Zhang, *et al.*, “Overlap Communication with Dependent Computation via Decomposition in Large Deep Learning Models,” in *ACM ASPLOS*, 2022.

[45] “Google vit-huge.” <https://huggingface.co/google/vit-huge-patch14-224-in21k>, 2024.

[46] “Stable diffusion 2.1.” <https://huggingface.co/stabilityai/stable-diffusion-2-1>, 2024.

[47] L. Zheng, Z. Li, H. Zhang, Y. Zhuang, Z. Chen, Y. Huang, Y. Wang, Y. Xu, D. Zhuo, E. P. Xing, *et al.*, “Alpa: Automating inter-and {Intra-Operator} parallelism for distributed deep learning,” in *USENIX OSDI*, 2022.

[48] M. Wang, C.-c. Huang, and J. Li, “Supporting very large models using automatic dataflow graph partitioning,” in *EuroSys*, 2019.

[49] Z. Jia, M. Zaharia, and A. Aiken, “Beyond data and model parallelism for deep neural networks,” *Conference on Machine Learning and Systems*, 2019.

[50] S. Li, F. Xue, C. Baranwal, Y. Li, and Y. You, “Sequence parallelism: Long sequence training from system perspective,” *arXiv preprint arXiv:2105.13120*, 2021.

[51] J. Liu, J. H. Wang, and Y. Jiang, “Janus: A unified distributed training framework for sparse mixture-of-experts models,” in *ACM SIGCOMM*, 2023.

[52] N. Du, Y. Huang, A. M. Dai, S. Tong, D. Lepikhin, Y. Xu, M. Krikun, Y. Zhou, A. W. Yu, O. Firat, *et al.*, “Glam: Efficient scaling of language models with mixture-of-experts,” in *International Conference on Machine Learning (ICML)*, 2022.

[53] S. Smith, M. Patwary, B. Norick, P. LeGresley, S. Rajbhandari, J. Casper, Z. Liu, S. Prabhumoye, G. Zerveas, V. Korthikanti, *et al.*, “Using deepspeed and megatron to train megatron-turing nlg 530b, a large-scale generative language model,” *arXiv preprint arXiv:2201.11990*, 2022.

[54] Y. Zhao, A. Gu, R. Varma, L. Luo, C.-C. Huang, M. Xu, L. Wright, H. Shojanazeri, M. Ott, S. Shleifer, *et al.*, “Pytorch fsdp: experiences on scaling fully sharded data parallel,” *arXiv preprint arXiv:2304.11277*, 2023.

[55] K. Qian, Y. Xi, J. Cao, J. Gao, Y. Xu, Y. Guan, B. Fu, X. Shi, F. Zhu, R. Miao, *et al.*, “Alibaba hpn: A data center network for large language model training,” 2024.

[56] C. Chen, X. Li, Q. Zhu, J. Duan, P. Sun, X. Zhang, and C. Yang, “Centauri: Enabling efficient scheduling for communication-computation overlap in large model training via communication partitioning,” in *ACM ASPLOS*, 2024.

[57] Q. Hu, Z. Ye, Z. Wang, G. Wang, M. Zhang, Q. Chen, P. Sun, D. Lin, X. Wang, Y. Luo, *et al.*, “Characterization of large language model development in the datacenter,” in *USENIX NSDI*, 2024.

[58] S. Athlur, N. Saran, M. Sivathanu, R. Ramjee, and N. Kwatra, “Varuna: scalable, low-cost training of massive deep learning models,” in *EuroSys*, 2022.

[59] J. Thorpe, P. Zhao, J. Eyolfson, Y. Qiao, Z. Jia, M. Zhang, R. Netravali, and G. H. Xu, “Bamboo: Making preemptible instances resilient for affordable training of large dnns,” in *USENIX NSDI*, 2023.

[60] I. Jang, Z. Yang, Z. Zhang, X. Jin, and M. Chowdhury, “Oobleck: Resilient distributed training of large models using pipeline templates,” in *ACM SOSP*, 2023.

[61] A. Radford, J. W. Kim, C. Hallacy, A. Ramesh, G. Goh, S. Agarwal, G. Sastry, A. Askell, P. Mishkin, J. Clark, *et al.*, “Learning transferable visual models from natural language supervision,” in *International conference on machine learning*, 2021.

[62] X. Zhai, X. Wang, B. Mustafa, A. Steiner, D. Keysers, A. Kolesnikov, and L. Beyer, “Lit: Zero-shot transfer with locked-image text tuning,” in *IEEE Conference on Computer Vision and Pattern Recognition*, 2022.

[63] J. Huang, Z. Zhang, S. Zheng, F. Qin, and Y. Wang, “Distmm: Accelerating distributed multimodal model training,” in *USENIX NSDI*, 2024.

[64] B. Jeon, M. Wu, S. Cao, S. Kim, S. Park, N. Aggarwal, C. Unger, D. Arfeen, P. Liao, X. Miao, *et al.*, “Graphpipe: Improving performance and scalability of dnn training with graph pipeline parallelism,” *arXiv preprint arXiv:2406.17145*, 2024.

[65] G.-I. Yu, J. S. Jeong, G.-W. Kim, S. Kim, and B.-G. Chun, “Orca: A distributed serving system for {Transformer-Based} generative models,” in *USENIX OSDI*, 2022.

[66] B. Wu, Y. Zhong, Z. Zhang, G. Huang, X. Liu, and X. Jin, “Fast distributed inference serving for large language models,” *arXiv preprint arXiv:2305.05920*, 2023.

[67] Y. Sheng, S. Cao, D. Li, B. Zhu, Z. Li, D. Zhuo, J. E. Gonzalez, and I. Stoica, “Fairness in serving large language models,” in *USENIX OSDI*, 2024.

[68] Y. Zhong, S. Liu, J. Chen, J. Hu, Y. Zhu, X. Liu, X. Jin, and H. Zhang, “Distserve: Disaggregating prefill and

decoding for goodput-optimized large language model serving,” in *USENIX OSDI*, 2024.

- [69] P. Patel, E. Choukse, C. Zhang, A. Shah, Í. Goiri, S. Maleki, and R. Bianchini, “Splitwise: Efficient generative llm inference using phase splitting,” in *ACM/IEEE ISCA*, 2024.
- [70] W. Kwon, Z. Li, S. Zhuang, Y. Sheng, L. Zheng, C. H. Yu, J. Gonzalez, H. Zhang, and I. Stoica, “Efficient memory management for large language model serving with pagedattention,” in *ACM SOSP*, 2023.
- [71] C. Jin, Z. Zhang, X. Jiang, F. Liu, X. Liu, X. Liu, and X. Jin, “Ragcache: Efficient knowledge caching for retrieval-augmented generation,” *arXiv preprint arXiv:2404.12457*, 2024.
- [72] L. Zheng, L. Yin, Z. Xie, J. Huang, C. Sun, C. H. Yu, S. Cao, C. Kozyrakis, I. Stoica, J. E. Gonzalez, *et al.*, “Efficiently programming large language models using sclang,” *arXiv preprint arXiv:2312.07104*, 2023.